Magnon sidebands and spin-charge coupling in bismuth ferrite probed by nonlinear optical spectroscopy

M. O. Ramirez,[1] A. Kumar,[1] S. A. Denev,[1] N. J. Podraza,[1,2] X. S. Xu,[3] R. C. Rai,[3] Y. H. Chu,[4,5] J. Seidel,[4,5] L. W. Martin,[4] S.-Y. Yang,[4] E. Saiz,[4] J. F. Ihlefeld,[2,4] S. Lee,[6] J. Klug,[7,8] S. W. Cheong,[6] M. J. Bedzyk,[7,8] O. Auciello,[8] D. G. Schlom,[1] R. Ramesh,[4,5] J. Orenstein,[5] J. L. Musfeldt,[3] and V. Gopalan[1]

[1]*Department of Materials Science and Engineering and Materials Research Institute, Pennsylvania State University, University Park, Pennsylvania 16802, USA*

[2]*Department of Electrical Engineering and Materials Research Institute, Pennsylvania State University, University Park, Pennsylvania 16802, USA*

[3]*Department of Chemistry, University of Tennessee, Knoxville, Tennessee 37996, USA*

[4]*Materials Sciences Division, Lawrence Berkeley National Laboratory, Berkeley, California 94720, USA*

[5]*Department of Physics, University of California, Berkeley, California 94720-1760, USA*

[6]*Department of Physics and Astronomy Rutgers and Rutgers Center of Emergent Materials, The State University of New Jersey, 136 Frelinghuysen Road, Piscataway, New Jersey 08854-8019, USA*

[7]*Materials Research Center, Northwestern University, Evanston, Illinois 60208, USA*

[8]*Materials Science Division, Argonne National Laboratory, Argonne, Illinois 60439, USA*

(Received 22 January 2009; revised manuscript received 27 March 2009; published 5 June 2009)

The interplay between spin waves (magnons) and electronic structure in materials leads to the creation of additional bands associated with electronic energy levels which are called magnon sidebands. The large difference in the energy scales between magnons (meV) and electronic levels (eV) makes this direct interaction weak and hence makes magnon sidebands difficult to probe. Linear light absorption and scattering techniques at low temperatures are traditionally used to probe these sidebands. Here we show that optical second-harmonic generation, as the lowest-order nonlinear process, can successfully probe the magnon sidebands at room temperature and up to 723 K in bismuth ferrite, associated with large wave vector multimagnon excitations which linear absorption studies are able to resolve only under high magnetic fields and low temperatures. Polarized light studies and temperature dependence of these sidebands reveal a spin-charge coupling interaction of the type $P_s L^2$ between the spontaneous polarization (P_s) and antiferromagnetic order parameter, L in bismuth ferrite, that persists with short-range correlation well into the paramagnetic phase up to high temperatures. These observations suggest a broader opportunity to probe the collective spin-charge-lattice interactions in a wide range of material systems at high temperatures and electronic energy scales using nonlinear optics.

DOI: 10.1103/PhysRevB.79.224106 PACS number(s): 78.20.Ls, 42.65.Ky, 42.70.Mp, 78.47.Fg

I. INTRODUCTION

The 1965 discovery and identification of magnon sidebands in the linear optical-absorption spectrum of simple antiferromagnetic insulators contributed to a comprehensive understanding of the static and dynamical optical properties of ordered magnetic systems.[1,2] These studies were based on the resonant enhancement of the susceptibility, $\chi_{ij}^{(1)}$, that appears in the linear interaction $P_i^{\omega}=\chi_{ij}^{(1)}E_j^{\omega}$.One can generally express $\chi_{ij}^{(1)}$ as

$$\chi_{ij}^{(1)}(\omega) \sim \frac{N}{\hbar}\sum_n \left[\frac{\mu_{an}^i \mu_{na}^j}{(\omega_{na}-\omega)-i\gamma_{na}}\right], \qquad (1)$$

where P_i^{ω} is the linear polarization at frequency ω, E_j^{ω} the electric field of light, N is the atomic number density, μ_{an}^i is the i-polarized dipole moment for transition from level n to a, and γ_{na} is the damping coefficient related to the resonance between levels n and a.[3] Therefore, when electric-dipole-active magnetic excitations couple to electronic excitations, magnon sidebands are located at $E_n=E_e \pm n\hbar M$, where $\hbar M$ is a single-magnon energy, n is the number of magnons assisting the transition, and E_e corresponds to the electronic crystal-field transitions.

In principle, the creation of a nonlinear polarization, $P_i^{2\omega}=\chi_{ijk}^{(2)}E_j^{\omega}E_k^{\omega}$ at a frequency 2ω, from two incident photons of frequency ω, should also reflect the presence of such magnon sidebands. With the rapid development of modern lasers, second-harmonic generation (SHG), as the lowest-order nonlinear optical process, has emerged as a powerful tool to study light-matter interactions. The highly restrictive symmetry rules for $\chi_{ijk}^{(2)}$, combined with its temperature and spectral dependences, can permit a differentiation between polar, magnetic, lattice rotation, and chiral phenomena in matter—characteristics of many modern materials.[4–8] However, while a vast majority of literature in nonlinear spectroscopy of magnetic materials rely on symmetry distinctions in $\chi_{ijk}^{(2)}$ between crystallographic and magnetic symmetries, such distinctions are not always present in all magnetic systems. Here, we show that even in such cases, SHG spectroscopy can be used to probe a more general feature present in all magnetic systems, namely, magnon sidebands to electronic levels.

Magnon sidebands of electronic excitations constitute the most direct manifestation of a prominent coupling between magnons and the linear susceptibility $\chi_{ij}^{(1)}$ in the system, a phenomenon generally expected to be weak because of the large energy difference between the electronic and magnetic excitations. In our work, we show that in a magnetically ordered system, spin waves can also effectively couple to the nonlinear susceptibility $\chi_{ijk}^{(2)}$ tensor. These collective interac-

tions are visualized as magnon sidebands of electronic excitations using nonlinear optical SHG spectroscopy. Moreover, the room-temperature (RT) detection of magnon sidebands in $BiFeO_3$, a room-temperature multiferroic material, in the form of coupling between magnons and electronic states via $\chi^{(2)}_{ijk}$ opens up a new approach to studying magnetoelectric interaction in multiferroic compounds at high temperatures and electronic energy scales.

In general spin-charge-lattice coupling in multiferroics occurs through interactions between magnons, electronic levels, and phonons. Of these interactions, only the magnon-phonon interactions are widely studied in multiferroics[9–11] and the interactions between magnons and electronic levels (magnon sidebands) as well as phonons and electronic levels (phonon sidebands) are unexplored thus far in multiferroics. A common signature of the electromagnetic coupling at finite frequencies in multiferroic materials is the presence of electromagnons, which are magnons that possess an electric-dipole moment due to the transfer of the electric-dipole spectral weight from phonons or electronic states. Recent works[10,11] on low-energy Raman-scattering experiments in $BiFeO_3$ have shown a strong interaction between optical phonons and magnons manifested as several sharp resonances (up to 12 peaks in the $5-60\ \mathrm{cm}^{-1}$ energy range) corresponding to two species of electromagnon excitations (spin-wave excitations in and out of the cycloidal plane) with distinctive dispersive energy curves depending on their coupling to the electrical polarization. These findings demonstrated that the optical response of a multiferroic system can reveal important information about its magnetic excitations and phonons. However, due to the large difference in the energy scales between electronic levels (eV) and magnons or phonons (meV) the expected magnon sidebands and phonon sidebands have not been explored. As shown here, nonlinear optics allows us to probe magnon sidebands, providing additional insights into the nature of the dynamical magnetoelectric phenomena. In this work, we detect magnon sidebands involving zone-boundary high-energy magnons of energies 0.19 and 0.29 eV. (All other magnon and phonon energies are lower than these in this system.) We also show resonances at specific temperatures involving low-energy phonons, high-energy magnons, and electronic levels. However, the phonons involved are of energies ranging from $\sim 0.02-0.1$ eV, which is of the order of the linewidth of our magnon sidebands at room temperature and above. Hence no specific phonon assignments are made that could allow a direct comparison to the previous low-energy electromagnon studies.[9,10] In principle, this is possible if narrower linewidths can be obtained, perhaps at lower temperatures. The SHG studies, however, do reveal information about the nature of polarization-antiferromagnetism coupling, namely, P_sL^2.

More specifically, let us assume three electronic levels participate in the SHG process. We define a ground-state energy E_a plus two higher-energy levels E_{b_n} and E_{c_n}. Here, we index sidebands with an additional subscript. For instance, sidebands of electronic level E_b are denoted as E_{b_n}. Further, assume that E_{b_n}-E_a (denoted as $E_{b_n a}$) and E_{c_n}-E_{b_n} (denoted as $E_{c_n b_n}$) are both nearly resonant with $\hbar\omega$, and E_{c_n}-E_a (denoted as $E_{c_n a}$) is nearly resonant with $2\hbar\omega$, as is relevant to this study. The nonlinear susceptibility is then given by

$$\chi^{(2)}_{ijk} = \frac{N}{2\hbar^2}\sum_n \left\{ \Delta\rho_{ab_n}\left[\frac{\mu^i_{ac_n}\mu^j_{c_n b_n}\mu^k_{b_n a}}{(\omega_{c_n a} - 2\omega - i\gamma_{c_n a})(\omega_{b_n a} - \omega - i\gamma_{b_n a})} \right] + \Delta\rho_{c_n b_n}\left[\frac{\mu^i_{ac_n}\mu^j_{c_n b_n}\mu^k_{b_n a}}{(\omega_{c_n a} - 2\omega - i\gamma_{c_n a})(\omega_{c_n b_n} - \omega - i\gamma_{c_n b_n})} \right] \right\}, \tag{2}$$

where the sum is over all the sidebands n and $\Delta\rho_{ab_n}$ indicates the population difference between the levels E_a and E_{b_n}. Other definitions are similar to those in Eq. (1). It is clearly seen that the SHG susceptibility, $\chi^{(2)}_{ijk}$, will reveal the magnon sidebands when the incident photon frequency ω (or its harmonic, 2ω) is resonant with the magnon levels $\omega_{b_n a}$ or $\omega_{c_n b_n}$ ($\omega_{c_n a}$). Magnon sidebands have been extensively studied by linear spectroscopy.[12–16] Magnetic SHGs based on time and spatial inversion symmetry distinctions,[4,17] Kerr rotation,[18] and nonlinear photoinduced absorption spectroscopy[19] have been used to study magnetic structures and spin-wave dynamics. However, to the best of our knowledge, magnon sidebands have not been reported by nonlinear optical spectroscopy, such as SHG. There are several interesting and unique aspects to the observations presented here. First, although magnon sidebands were recently observed in the linear magneto-optical absorption spectrum of $BiFeO_3$ under high magnetic fields and low temperatures,[20] nonlinear optical spectroscopy has the potential to provide greater sensitivity for the study of these sidebands at high temperatures and no magnetic fields. Second, we observe the sidebands in the nonlinear spectrum of $BiFeO_3$ at room temperature and even up to 723 K. In comparison, most magnon sidebands reported in literature using linear absorption measurements are at low temperatures.[12–15] Third, magnon sidebands allow us to directly probe spin-charge coupling in multiferroic $BiFeO_3$ through a coupling of the nonlinear optical susceptibility to the term P_sL^2, where P_s is the polarization and L is the antiferromagnetic order parameter. Finally, the technique provides an alternative to neutron diffraction for probing many magnetic systems, especially in thin-film form.

II. ELECTRONIC ENERGY LEVELS IN BISMUTH FERRITE

Bismuth ferrite, $BiFeO_3$, the focus of this study, shows a robust ferroelectric polarization ($P_s \sim 100\ \mu\mathrm{C/cm}^2$) at room temperature[21] that is the largest among known ferroelectrics. At 300 K, $BiFeO_3$ is a rhombohedrally distorted ferroelectric perovskite with space group $R3c$ and a Curie temperature, $T_C \sim 1100$ K.[22] It also shows a G-type canted antiferromagnetic order below Néel temperature, $T_N \sim 640$ K, and, in the bulk, an incommensurately space-modulated spin structure along $(110)_h$.[23] Several physical properties have been reported to show anomalies across T_N,[24–26] pointing toward the importance of spin-charge-lattice coupling mechanisms. Additionally, its large unit cell suggests the presence of high-

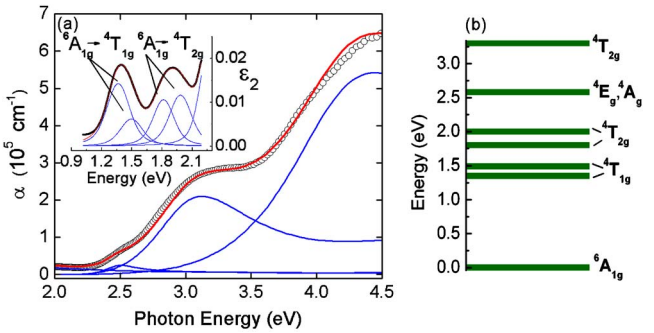

FIG. 1. (Color online) (a) The 300 K absorption spectrum obtained from a 100 nm thick $BiFeO_3$ film and (inset) a 67 μm thick $BiFeO_3$ single crystal. Solid lines are linear oscillator fits using a parameterized dielectric function consisted of three Tauc-Lorentz oscillators sharing a common gap (Ref. 30), a Lorentz oscillator (Ref. 31), and a constant additive term to ε_1. (Blue: component fits, Red: total fit.) (b) Schematic electronic energy-level diagram of Fe^{3+} in $BiFeO_3$ derived from these measurements.

energy spin-wave optical branches, as previously observed in other iron oxides,[27] making this material especially suitable for the study of magnon sidebands by means of nonlinear optical spectroscopy.

To probe the coupling between spin and charge in $BiFeO_3$, we first establish its electronic energy-level scheme by means of linear absorption spectroscopy measured between 5 and 730 K. Electronic structure investigations have already established the strongly hybridized nature of the valence bands,[28,29] and although the mixing of Fe^{3+} d levels with O p and Bi s states fundamentally impacts the chemical bonding, it does not change the symmetry of the crystal-field-derived bands. Therefore, in the interest of clarity, the electronic structure will be discussed using traditional ligand field terminology, but with the realization that these states are strongly hybridized. In particular, by considering the C_{3v} local symmetry of Fe^{3+} ions in $BiFeO_3$ and using the correlation group and subgroup analysis for the symmetry breaking from O_h to C_{3v}, up to six d to d excitations are expected for $Fe^{3+}(3d^5)$ ions between 0 and 3 eV. Note that the triply degenerate $^4T_{1g}$ and $^4T_{2g}$ electronic levels split into two crystal-field levels with A and E characters due to the symmetry reduction. The inset in Fig. 1(a) shows a close-up view of the absorption spectrum obtained on a 67 μm thick $(10\bar{1}2)$ oriented single crystal. Between 1 and 2.2 eV, the spectrum displays two broad absorption bands which, based on the four predicted (but spin-forbidden) on-site d-to-d crystal-field excitations of Fe^{3+} ions in this energy range, can be resolved into four different linear oscillator components [imaginary part of $\chi_{ij}^{(1)}$ in Eq. (1)].[20] Above 2.2 eV, the absorption increases substantially. As a result, measurements were also carried out on thin-film samples (0001)-oriented single-crystalline $BiFeO_3$ grown by molecular-beam epitaxy on (111) $SrTiO_3$ substrates. Figure 1(a) shows the thin-film absorption spectrum obtained at 300 K. It displays an onset at ~2.2 eV, a small shoulder centered at ~2.45 eV, and two larger features near 3.2 and 4.5 eV that are assigned as charge-transfer excitations.[28,29] The charge gap is observed at 2.66 eV at 300 K. The features above or near the charge gap can be assigned as a combination of charge-transfer excitations, higher-energy crystal-field excitations, and (possibly) double-exciton features such as at ~2.45 eV. Crystal-field levels cannot be distinguished from charge transfer and excitonic bands in the linear spectra above ~2.2 eV because their intensity is weak compared to the other features. Nonetheless, the positions of ^4E_g and ^4A_g crystal-field levels for Fe^{3+} in a C_{3v} environment are expected to be slightly below the ~2.6 eV, which is the calculated crystal-field level for Fe^{3+} in a cubic environment.[32] Using the SHG spectra discussed later on, we locate a crystal-field level at ~2.56 eV. Similarly, the position of the $^4T_{2g}$ level of Fe^{3+} in a C_{3v} environment is expected to be slightly below ~3.4 eV, which is the calculated crystal-field level in a cubic environment. Hence we assign it to be ~3.3 eV. From this analysis, the resulting electronic energy-level scheme for the Fe^{3+} ion is shown in Fig. 1(b) and summarized in Table I.

III. HIGH-ENERGY MULTIMAGNONS IN BISMUTH FERRITE

High-energy zone-boundary magnon energies relevant to this study were experimentally determined by Raman and midinfrared absorption experiments. Figure 2(a) shows a detail of the 300 K Raman spectrum in $BiFeO_3$ recorded in the

TABLE I. Relevant energy levels of $BiFeO_3$ at 296 K.

Type of energy levels	Energies (eV)
Crystal-field levels of Fe^{3+} in $BiFeO_3$	1.36, 1.48, 1.79, 1.99, 2.56, ~3.3
Multimagnon energies	$2M\sim0.19$, $3M\sim0.29$
Observed crystal SHG electronic (e) resonances	1.36, 1.48, 2.56
Observed crystal SHG magnon (m) resonances	2.56+2M, 2.56+3M, (3.3−2M, 1.36+2M, 1.48 +1M) The bracketed resonances are close in energy and observed as the 3.14 ± 0.05 eV magnon resonance in Fig. 3(a).
Double-exciton/charge-transfer bands	~2.45, ~3.2, ~4.5
Charge gap, E_g	2.66

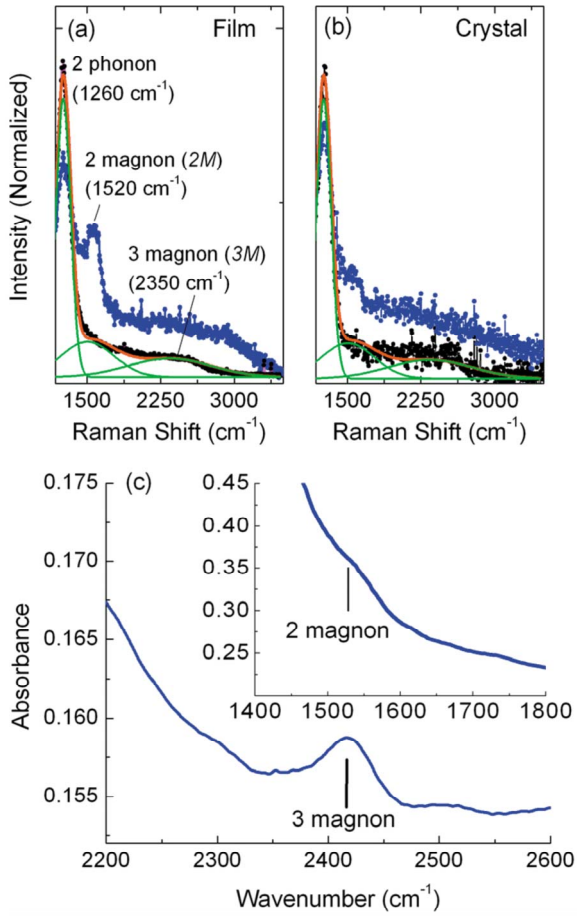

FIG. 2. (Color online) Room-temperature unpolarized Raman spectra of (a) a 4.5 μm thick $(10\bar{1}2)$-oriented epitaxial $BiFeO_3$ film grown on a (110) $DyScO_3$ substrate and (b) a $(10\bar{1}2)$-oriented single crystal. The experimental data in black is at 296K and in blue is at $T_1^*=365$ K, where two-magnon peak shows resonant enhancement. The three Gaussian fits to RT spectra correspond to two-phonon, two-magnon, and three-magnon replicas, respectively, from low-to-high wave-number shift. (c) RT midinfrared linear absorption measured on a $BiFeO_3$ bulk single crystal. The energy positions of two- and three-magnon absorption bands have been marked in the figure.

high-frequency region where two- and three-magnon scatterings can be observed at the shoulder of the previously reported two-phonon overtone.[26] Further details on the temperature-dependent Raman spectra under 1300 cm^{-1} can be found in Refs. 24 and 33. Due to the lack of high-energy magnon dispersion curves for $BiFeO_3$, the two- and three-magnon assignments were made on the basis of the striking spectral similarity between $BiFeO_3$ and α-Fe_2O_3, the simplest case of an iron oxide containing only FeO_6 octahedra, where not only two-magnon scattering but also two-phonon overtones at very similar energies have been reported.[34] From the fitting, the energy values of two- and three-magnon excitations were found to be 1530 and 2350 cm^{-1}, respectively. The films and crystals were confirmed to be phase-pure $BiFeO_3$, with no secondary phases such α-Fe_2O_3, by using synchrotron x-ray diffraction and transmission electron microscopy. In addition, to confirm these assignments, room-temperature midinfrared absorption experiments were performed in the same energy range. The results are shown in Fig. 2(b) in which an absorption band centered at 2415 cm^{-1} is clearly resolved. The energy of this absorption band matches that obtained for three-magnon excitation from Raman-scattering experiments. At lower energies, the strong contribution to the absorption spectra of the second-order overtones precludes resolving the two-magnon absorption band, though its contribution around 1550 cm^{-1} is clearly appreciable [see inset in Fig. 2(b)]. The two-magnon peaks show resonant enhancement at specific temperatures as described elsewhere.[35] The peak position of the two-magnon peak is also relatively insensitive to temperature (shift of <0.03 eV) from 296 to 700 K.[35]

IV. OPTICAL SHG SPECTROSCOPY

Figure 3(a) shows the SHG spectra obtained in $BiFeO_3$ films,[36] bulk single crystal at 296 K, and for the crystal at 723 K. A tunable optical parametric oscillator (Spectra Physics MOPO) with 10 ns pulses was used for SHG experiments. For the comparison between different samples, an effective $|\chi_{ijk}|^2$ for different samples was determined by normalizing the SHG intensity with the square of the incident power, absorption spectrum of the fundamental and SHG signals, coherence length dispersion, and detector sensitivity at each wavelength as previously described.[37] The thin film used for SHG was a 50 nm thick (0001)-oriented single-crystalline $BiFeO_3$ grown by molecular-beam epitaxy on (111) $SrTiO_3$ substrates with no other twin or in-plane rotational variants.[36] Thus importantly, the film was single crystalline and single domain and allowed the SHG extraction of χ_{222}. The single-crystal samples employed in these experiments were $(10\bar{1}2)$ oriented and polydomain and thus resulted in a χ_{eff}.

Up to six different excitations are observed with maxima centered at ~2.56, 2.73, 2.79, 2.87, 2.95, and 3.14 eV. These energies are denoted by short vertical lines in the plot. It is clear that for the energy range analyzed in this work (1.23–1.65 eV for the pump beam and 2.46–3.3 eV for the second-harmonic spectra), a maximum of three electronic resonances is theoretically expected for the generated SHG signal. This prediction is in line with the observed spectral features at ~2.56 eV (SHG resonance) and ~2.73 and ~2.95 eV (fundamental resonances, $\omega=1.36$ and 1.48 eV, respectively). They are marked with red arrows in Fig. 3(b) and summarized in Table I. Below, we argue that the additional resonances at ~2.79, 2.87, and 3.14 eV can be explained in terms of multimagnon coupling to the electronic states in multiferroic $BiFeO_3$.

Figure 3(b) shows the electronic energy-level scheme when two- and three-magnon sidebands at $2\hbar M \sim 0.19 \pm 0.15$ eV and $3\hbar M \sim 0.29 \pm 0.15$ eV are considered. Other low-energy zone-center magnons observed in this material are not considered in the SHG spectrum analysis.[11] Thus, within the experimental error, the observed SHG transitions at 2.79 and 2.87 [marked with solid blue arrows in Fig. 3(b)] can be directly associated with $+2\hbar M$ and $+3\hbar M$ magnon energy levels above the electronic energy level $E_e=2.56$ eV. The weak shoulder observed at

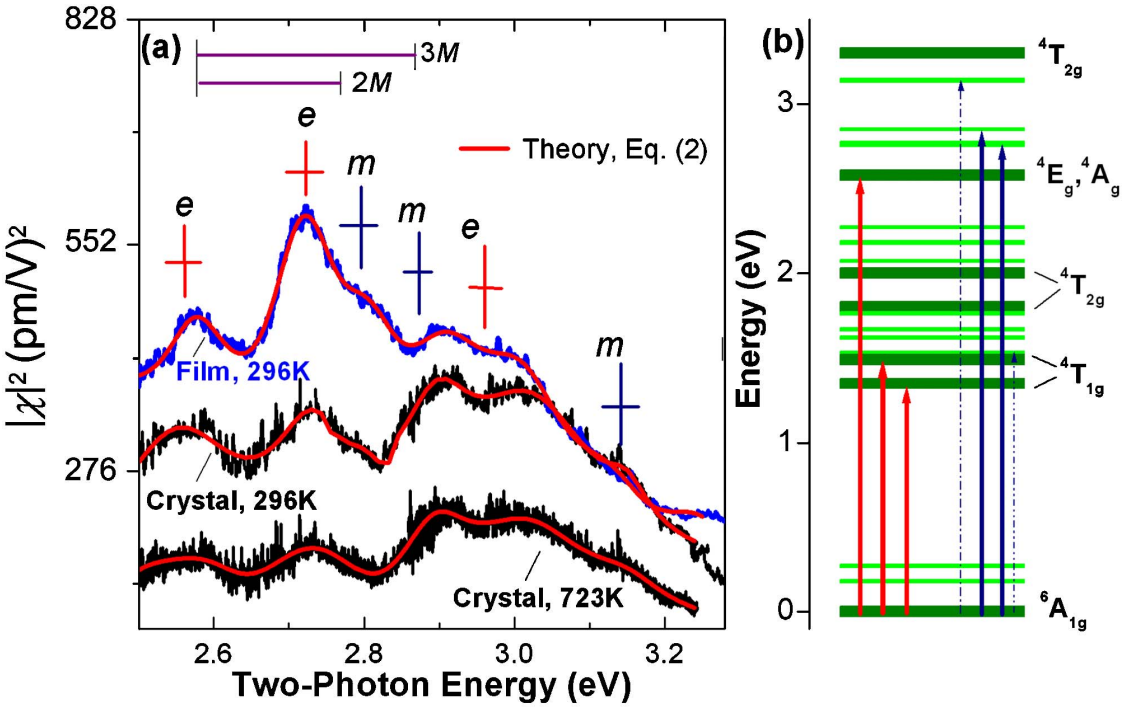

FIG. 3. (Color online) (a) RT SHG spectra obtained in $BiFeO_3$ film (black) and bulk single crystal (blue). Solid red lines show the theoretical fitting to Eq. (2). The parameters for theory fit for single crystal at 296 K are $\omega_{c_n a}=2.56\pm0.05$, 2.79 ± 0.05 eV, 2.87 ± 0.05, and 3.14 ± 0.05 eV, and $\omega_{b_n a}=1.36\pm0.05$ and 1.48 ± 0.05 eV, which are shown as red (electronic, e) and blue (magnon, m) crosses indicating mean energies and associated error bars. The theory parameters for single crystal at 723 K are $\omega_{c_n a}=2.61\pm0.05$, 2.84 ± 0.05, 2.90 ± 0.05, and 3.16 ± 0.05 eV, and $\omega_{b_n a}=1.37\pm0.05$ and 1.51 ± 0.05 eV. The theory parameters for the thin film at 296K are $\omega_{c_n a}=2.55\pm0.05$, 2.78 ± 0.05, 2.83 ± 0.05, and 3.16 ± 0.05 eV, and $\omega_{b_n a}=1.36\pm0.05$ and 1.51 ± 0.05 eV. In all cases, $\omega_{c_n b_n}=\omega_{c_n a}-\omega_{b_n a}$. The resonance linewidths for all these resonance fits were $\gamma=0.08\pm0.05$ eV. Purple horizontal scale bars of two-magnon ($2M$) and three-magnon ($3M$) energies separating e and m resonances are shown. (b) Electronic energy-level diagram of Fe^{3+} in $BiFeO_3$. Dark green bars: energy positions for the d to d excitations of Fe^{3+} ions in $BiFeO_3$. Light green bars: energy positions for two- and three-magnon sidebands. Arrows indicate the electronic (red) and magnon (blue) SHG resonances in $BiFeO_3$. Broken blue arrows suggest multiple possibilities for the 3.14 eV magnon resonance.

~3.14 eV is also related to magnon sidebands. Its energy position, shown by broken blue arrows in Fig. 3(b) matches $\sim -2\hbar M$ from the crystal-field level predicted at ~3.3 eV, $+2\hbar M$ from the electronic resonance at 1.36 eV, as well as $\sim +1\hbar M$ from the fundamental resonance at 1.48 eV, all of which can have contributions to this resonance shoulder. Therefore, the origin of the extra bands observed in the SHG wavelength scan can be explained in terms of spin-charge mixing with multiple magnons.

Indeed, fitting $|\chi_{ijk}|^2$ from Eq. (2), we can reproduce the key features of the observed crystal spectrum at 296 K by considering only the electronic (e) and magnon (m) resonance terms corresponding to $\omega_{c_n a}=2.56\pm0.05$ eV(e), 2.79 ± 0.05 eV(m), 2.87 ± 0.05 eV(m), and 3.14 ± 0.05 eV(m), $\omega_{b_n a}=1.36\pm0.05$ eV(e) and 1.48 ± 0.05(e), and $\omega_{c_n b_n}=\omega_{c_n a}-\omega_{b_n a}$. The theory fits in Fig. 3(a) were calculated as follows. Considering two fundamental resonances, $\omega_{b_n a}$, and four second-harmonic resonances, $\omega_{c_n a}$, in Eq. (2), one would expect eight terms in the summation of Eq. (2). To manage the total number of independent variables, the following reasonable assumptions were made: The amplitudes and linewidths (γ) of the two close fundamental resonances $\omega_{b_n a}$ were assumed equal. The linewidths (but not the amplitudes) of the fundamental resonances $\omega_{b_n a}$ and $\omega_{c_n a}-\omega_{b_n a}$ were assumed equal. The fits shown are not unique; however, there is a limited region of frequencies and linewidths (indicated by the error bars) where the fits converge and are unstable outside, suggesting that the numerical values quoted for the frequencies and linewidths are robust within the error bars. We also note that the linewidths extracted from the theory fit are narrower than what one might expect in wrongly trying to resolve this spectrum into six simple peak functions. Each pair of terms in the summation of Eq. (2) would have spectral weight at three different resonance frequencies. The overall summation over eight such terms will have spectral weight at 12 such resonant wavelengths instead of only six one might naively expect. This leads to narrower SHG linewidths than the linear absorption spectra in Fig. 1.

The magnon sidebands are observed even up to 723 K, as shown, where multimagnon excitations in the form of pairs of very short wavelength spin waves at the zone boundary can persist well above T_N into the paramagnetic phase, as also previously reported in other systems.[38] Interestingly, the theory fit at 723 K suggests that these magnon levels are relatively insensitive to temperature (peak shift ~0.03 eV) in this temperature range, consistent with Raman

experiments.[39] A similar fit performed for the thin-film spectrum at 296 K in Fig. 3 agrees very well with the extracted single-crystal resonance frequencies and linewidths. The primary differences in the SHG spectrum between the single crystal and the thin film come from the amplitudes of the various susceptibility terms in Eq. (2). This is expected, since the effective χ_{ijk} for the $(10\bar{1}2)$ oriented single crystal is a mixture of various SHG tensor components in the geometry studied, while the (0001)-oriented thin-film signal primarily arises from the χ_{222} term. We note that the electronic resonances at ~1.36 and ~1.48 eV considerably overlap in the linear spectra of Fig. 1, while they are clearly separated in the SHG spectra of Fig. 3 (as 2.73 and 2.95 eV peaks). This highlights a natural advantage of the SHG process, where the peak separations double relative to the linear optical spectra. Significantly, this feature of SHG enables the detection of magnon sidebands at ~2.79 and 2.87 eV between these electronic levels. Another advantage of SHG spectroscopy arises from the narrow resonance linewidths. In this work, we found typical SHG experimental linewidths obtained from the theoretical fit to Eq. (2) to be $\gamma \sim 80$ meV at ~300 K. In contrast, the linear absorption linewidths of the crystal-field resonances [inset of Fig. 1(a)] are ~3 times broader.

Further evidence that the SHG fine structures in $BiFeO_3$ are magnon sidebands comes from polarization studies and the temperature dependence of these features. Interestingly, the SHG polar plots shown in Fig. 4(a) consistently indicate polar $3m$ point-group symmetry over the entire temperature range and photon energies studied in this work as seen from the excellent theoretical fits of these data to the equations

$$I_{\parallel} = \chi_{222}^2 \sin^2 3\phi, \quad I_{\perp} = \chi_{222}^2 \cos^2 3\phi, \tag{3}$$

where $I_{\parallel}$ and $I_{\perp}$ represent the SHG intensity collected in normal incidence with the fundamental (frequency ω) and second-harmonic (2ω) optical polarizations parallel and perpendicular to each other, respectively, χ_{222} refers to the relevant nonlinear optical coefficient, and ϕ is the angle of the incident polarization direction from the crystallographic x $[2\bar{1}\bar{1}0]$ direction. The polarization angles, ϕ, where the SHG signal is precisely zero, are very narrow in angle ($\Delta\phi \sim 0.01°$) and robust against temperature, magnetic fields (up to 2 Tesla), different samples, and sample regions. This clearly indicates that the observed $3m$ symmetry is an intrinsic effect. The large amplitude of SHG signals ($\chi_{ijk} \sim 298$ pm/V) (Ref. 37) and a significant enhancement of the signal below the T_N indicate that the dominant SHG interaction is the electric-dipole interaction, $P_i^{2\omega} = \chi_{ijk} E_j^{\omega} E_k^{\omega}$, with the susceptibility tensor, χ_{ijk}, exhibiting $3m$ symmetry and strongly coupled to the on-site spin vector $\boldsymbol{S}$. Figure 4(b) shows the temperature dependence of the SHG recorded at two different energies: 2.85 eV, nearly resonant with a multimagnon sideband [Fig. 2(b)], and 1.68 eV, which is far away from the resonant spectral range. For the nonresonant excitation energy, the temperature evolution of the SHG signal remains relatively featureless up to 725 K. In contrast, when the SHG process is magnon assisted (2.85 eV), a strong intensity decreases on approaching T_N. This reduction is recovered on cooling and strongly suggests a coupling between magnetism and the induced nonlinear polarization $P_i^{2\omega}$.

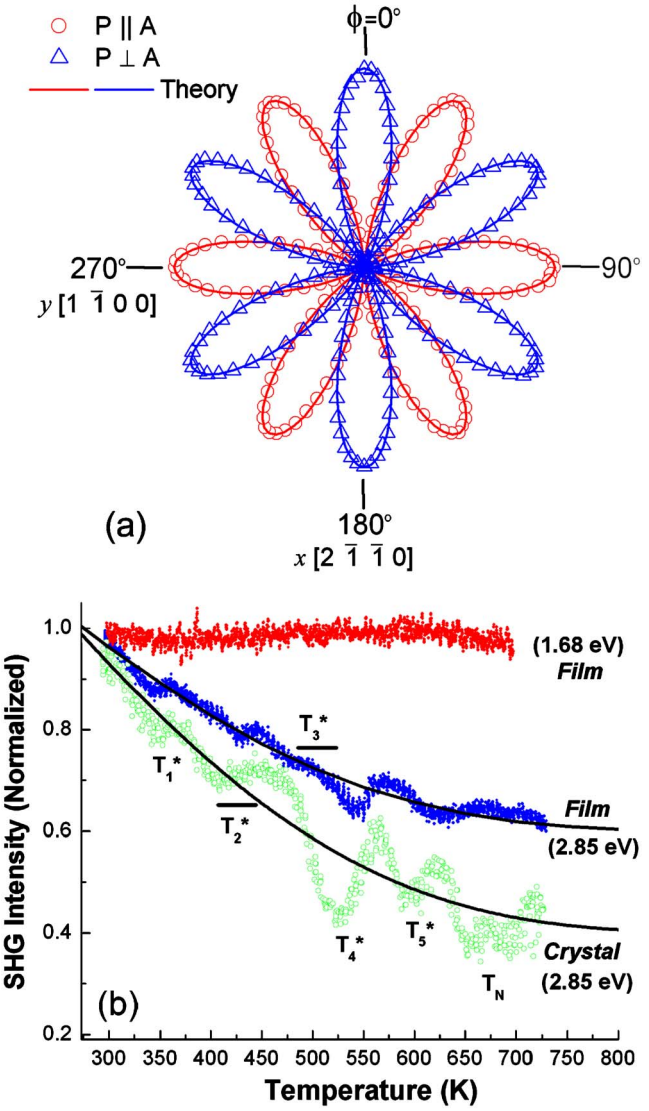

FIG. 4. (Color online) (a) The variation of the SHG intensities $I_{\parallel}$ (circles) and $I_{\perp}$ (triangles) with incident polarization angle, ϕ, measured at normal incidence and 300 K in a single-crystal quality (0001) $BiFeO_3$ thin film on $SrTiO_3$ (111) substrate. Solid lines are theoretical fits obtained from Eq. (3). (b) Optical SHG vs temperature for thin film and bulk single crystal recorded at two different energies: 2.85 eV (resonant transition) and 1.68 eV (nonresonant transition). Solid lines are theory fits from Eq. (7) with $T_o \sim 982$ K for film data and $T_o \sim 986$ K for the crystal data.

V. DISCUSSION OF THE SPIN-CHARGE COUPLING IN BISMUTH FERRITE

The fact that the SHG signal reveals a robust polar $3m$ symmetry at *all temperatures* and *all wavelengths* studied in this work is striking. Further, considering that the SHG signal dramatically increases as a power law with temperature below the T_N reveals a strong coupling to the spin order parameter, $\boldsymbol{S}$. This increase, however, is not accompanied by

any deviation in symmetry from $3m$ in the SHG signal. These observations reveal a simple and elegant coupling term between the SHG optical fields and the spontaneous polarization and spin order parameters of the system that robustly exhibits the $3m$ symmetry at all wavelengths and temperatures, even across T_N. We calculate this coupling term to the lowest order next.

The antiferromagnetic order parameter is $\boldsymbol{L}=\boldsymbol{S}_A-\boldsymbol{S}_B$ and the weak magnetism due to canting $\boldsymbol{M}=\boldsymbol{S}_A+\boldsymbol{S}_B$, where $\boldsymbol{S}_A$ and $\boldsymbol{S}_B$ are spins on adjacent Fe atoms along the c axis. $\boldsymbol{L}$ is a polar vector, while $\boldsymbol{M}$ is an axial vector, and both are antisymmetric with respect to time-reversal symmetry, $1'$. The spontaneous polarization vector, $\boldsymbol{P}_s$, is polar and time symmetric.

Starting from an appropriate prototype phase of $\bar{3}m1'$ for $BiFeO_3$,[40] one can derive the relevant coupling terms in the low-temperature ferroelectric, antiferromagnetic phase. The detailed theory for deriving various SHG coupling terms based on Ginzburg-Landau theory is given by Sa *et al.*[41] We note that in Ginzburg-Landau theory, all the order parameters and any coupling term involving them in the low-temperature multiferroic phase must have a physical mechanism by which they can evolve from the high-temperature high-symmetry nonmultiferroic prototype phase. This means that there must be appropriate energy terms in the prototype phase that are invariant with the symmetry elements of that phase, which naturally evolve through the intermediate phase transitions to give rise to the appropriate coupling terms in the low-temperature phase as one or more order parameters become finite in that phase. For example, the third-rank piezoelectric tensor property, d_{ijk}, in a ferroelectric phase actually evolves from a fourth-ranked electrostriction tensor, γ_{ijkl}, in the high-temperature nonferroelectric phase when biased by the spontaneous ferroelectric polarization, P_s, which becomes finite below the phase transition. Thus an appropriate electrostrictive energy term of the general form $\gamma_{ijkl}\varepsilon_{ij}P_kP_l$ that is symmetry invariant in the high-temperature phase (prototype phase) must exist, where ε_{ij} is the strain tensor. Similarly, the generalized Ginzburg-Landau functional from which the nonlinear optical susceptibility tensor is derived has to obey the symmetry of the high-temperature phase as the breakdown of the symmetry is inherent in the solution which is a minimum of the Ginzburg-Landau functional.

For example, let us consider the case of SHG arising below T_c in $BiFeO_3$ due to breaking of the inversion symmetry due to the transition to a ferroelectric phase. From the symmetry of the susceptibility tensor in the paraelectric phase ($\bar{3}m1'$) and that of the spontaneous polarization, $P_3=P_s$, along the threefold axis, we can write down the appropriate free-energy expression of the form

$$F=-[\chi_{ijk3}(T>T_c)E_i^{2\omega}E_j^{\omega}E_k^{\omega}]P_3^0. \tag{4}$$

Note that a fourth-rank polar tensor is allowed in the centrosymmetric prototype phase and the above energy term is invariant under the symmetry operations of the prototype phase point group. The spontaneous polarization is zero in the prototype phase. However, as the temperature is lowered below the ferroelectric phase transition, P_3 becomes nonzero and this energy term becomes the source for the third-order SHG susceptibility given by

$$\chi_{ijk}(T<T_c)=\chi_{ijk3}(T>T_c)P_3. \tag{5}$$

From the symmetry analysis of this fourth-rank tensor, one gets the nonzero components of $\chi_{ijkl}(T>T_c)$ in the paraelectric phase, which when contracted with the order parameter P_3 (i.e., $l=3$), gives rise to all the nonzero components of $\chi_{ijk}(T<T_c)$ in the ferroelectric phase given as

$$\chi_{ijk}(T<T_c)=\begin{pmatrix} 0 & 0 & 0 & 0 & \chi_{131} & -\chi_{222} \\ -\chi_{222} & \chi_{222} & 0 & \chi_{131} & 0 & 0 \\ \chi_{311} & \chi_{311} & \chi_{333} & 0 & 0 & 0 \end{pmatrix}. \tag{6}$$

This is precisely the form of the SHG tensor for the $3m$ symmetry in the ferroelectric phase and confirms the Ginzburg-Landau methodology outlined above and in Ref. 41. This determines the SHG signal $I_{FE}^{2\omega}$ in the ferroelectric-paramagnetic phase. It follows from the above expression that the SHG susceptibility in the ferroelectric phase is a linear function of the ferroelectric order parameter, P_s.

For spin coupling to SHG signal, we can eliminate linear coupling to S, L, or M through a fourth-rank susceptibility tensor since such coupling is destroyed by the $1'$ symmetry in the prototype phase. Explicitly, the relevant lowest-order energy term would be of the form $F=-[\chi_{ijkl}(T>T_c)E_i^{2\omega}E_j^{\omega}E_k^{\omega}]S_l$ and similarly for L and M. Such a term would be noninvariant under the time-reversal symmetry, $1'$, in the prototype phase. Coupling to P_s^2, S^2, L^2 through a fifth-rank susceptibility tensor is destroyed by the $\bar{1}$ symmetry because the relevant energy terms $F=-[\chi_{ijklm}(T>T_c)E_i^{2\omega}E_j^{\omega}E_k^{\omega}]P_l^0P_m^0$, etc. are noninvariant with $\bar{1}$ symmetry of the prototype phase. Coupling to PS type terms through $F=-[\chi_{ijklm}(T>T_c)E_i^{2\omega}E_j^{\omega}E_k^{\omega}]P_lS_m$ is similarly disallowed by the $1'$ symmetry of the prototype phase.

Thus the lowest-order magnetic coupling allowed in this system is through a sixth-rank susceptibility energy term of the type $F=-[\chi_{ijklmn}(T>T_c)E_i^{2\omega}E_j^{\omega}E_k^{\omega}]P_l^0S_mS_n$ in the prototype phase. The SHG tensor arising from this coupling is $\chi_{ijk}(T<T_c)=\chi_{ijklmn}(T>T_c)P_l^0S_mS_n$. By applying Neumann's law, this tensor yields the correct $3m$ symmetry observed in our SHG experiments [same as Eq. (6)] when $m=n$, i.e., $\chi_{ijk}=\chi_{ijk311}P_3^0S_1^2$, and similarly for S_2^2 and S_3^2. In other words, terms of the type P_sS^2 are symmetry allowed to couple to the SHG signal starting from the prototype phase and yield the correct $3m$ symmetry of the SHG tensor. When $m\neq n$, the tensor represents coupling to terms of the cross product, $\boldsymbol{S}_1\times\boldsymbol{S}_2$, such as $\chi_{ijk}(T<T_c)=\chi_{ijklmn}(T>T_c)P_3^0S_1S_2$ and yields the following SHG tensor:

$$\chi_{ijk}(T<T_c)=\begin{pmatrix} \chi_{111} & \chi_{122} & \chi_{133} & \chi_{123} & 0 & 0 \\ 0 & 0 & 0 & 0 & \chi_{231} & \chi_{212} \\ 0 & 0 & 0 & 0 & \chi_{331} & \chi_{312} \end{pmatrix}. \tag{7}$$

This tensor form is clearly different from the experimentally observed SHG tensor and thus rules out SHG coupling in our

experiments to the Dzyaloshinskii-Moriya (DM) type interaction, which is proportional to $\boldsymbol{S}_A \cdot \boldsymbol{S}_B = (S_{1,A}S_{2,B} + S_{1,B}S_{2,A})\hat{z}$ that gives rise to spin canting and the weak magnetism, $\boldsymbol{M}$. Note that we are not ruling out the DM interaction by itself in the multiferroic phase, but rather its coupling to the SHG tensor that we are experimentally probing. To make that more explicit, one can have DM energy term[42] such as $F = -D_{ij}S_iS_j$, which is invariant with $\bar{3}m1'$ symmetries of the prototype phase, and will give rise to spin canting in the low-temperature antiferromagnetic phase. Interestingly, however, one cannot have energy terms of the type $F = -D_{ijk}P_iS_jS_k$ in the prototype phase since it is noninvariant with the $\bar{1}$ symmetry. However, when coupled to the SHG optical process as shown above, to the lowest order, the SHG signal does indeed arise from a PL^2 coupling to the SHG optical fields.

We also note that $\boldsymbol{L}^2 = \boldsymbol{S}_A^2 + \boldsymbol{S}_B^2 - 2\boldsymbol{S}_A \cdot \boldsymbol{S}_B$. The terms $S_{A,B}^2$ would involve a two-magnon excitation on one or the other spin sublattice only and light scattering would occur through second-order spin-orbit coupling. This is symmetry allowed, but typically weak.[43] The stronger interaction is through the $\boldsymbol{S}_A \cdot \boldsymbol{S}_B$ term, which involves a simultaneous excitation of one magnon on each spin sublattice and their exchange coupling. This leads to light scattering through an exchange-scattering mechanism similar to that proposed by Fleury and Loudon[44] for the Raman-scattering process. For example, an exchange-scattering event involving the SHG process can occur as the excitation of one electron to a magnon sideband level by two photons of frequency ω, with a simultaneous spin flip of this electron as well as a neighboring electron through the $S_A^- S_B^+$ spin operator (superscripts + and − indicate spin raising and lowering operations), which conserves the spin angular momentum. Finally, the excited electron returns to the orbital ground state emitting a SHG photon at frequency 2ω. Considering the temperature dependence of magnetization at low temperatures from the Bloch theory[45] and noting that the magnetic SHG intensity $I_{AFM}^{2\omega} \propto |P^{2\omega}|^2 \propto P_s^2 L^4$, one can expect a strong dependence of the magnetic contribution to SHG intensity versus temperature near T_N as

$$I_{AFM}^{2\omega} = I_o^{2\omega}[1 - (T/T_o)^{3/2}]^4. \tag{8}$$

The expression for the total intensity $I^{2\omega} = I_{FE}^{2\omega} + I_{AFM}^{2\omega}$ fits the experimental data well as shown in Fig. 4(b). A T_o value of ~980 K extracted from the fit for both the film and the crystal suggests that the coupling P_sL^2 due to zone-boundary two-magnon excitations can persist over very short correlation lengths in the paramagnetic phase well past the T_N and even up to the Curie temperature, T_c. This is consistent with the observation of spectral density in magnon sidebands even at 723K in Fig. 3(a).

We finally briefly note the SHG anomalies in both single crystal and thin-film samples at a series of temperatures below T_N: $T_1^* \sim 380$ K, $T_2^* \sim 410$ K, $T_3^* \sim 480$ K $T_4^* \sim 525$ K, $T_5^* \sim 595$ K, and $T_N \sim 650$ K, each with an error bar of $\sim \pm 25$ K. No anomalous behavior in the temperature dependence of the measured lattice parameters, resistivity, or magnetic susceptibility was observed at any of the $T_1^* - T_5^*$ temperatures, thus ruling out new magnetic phase transitions. However, we note in Fig. 5 that the energy difference between the temperature insensitive crystal-field level at 2.56 eV and the strongly temperature sensitive[46] $E_{shoulder} \sim 2.45$ eV is $\sim 1M$ at T_1^* and $\sim 2M$ at T_5^*. This suggests a possible mixing of the electronic levels at 2.45 and 2.56 eV mediated by magnons. A possible source of the anomalies in the SHG susceptibility can thus be the resonances between a magnon sideband at 2.56 eV-nM and a temperature-dependent electronic level at 2.45 eV (296 K) level. We note that low-energy phonons could be involved in this process, especially at the T_2^*, T_3^*, and T_4^* anomalies, since the energy separations between T_1^* and these transitions in terms of the corresponding shift in the energy of the electronic shoulder are on the order of the lattice energy (0.02–0.1 eV).

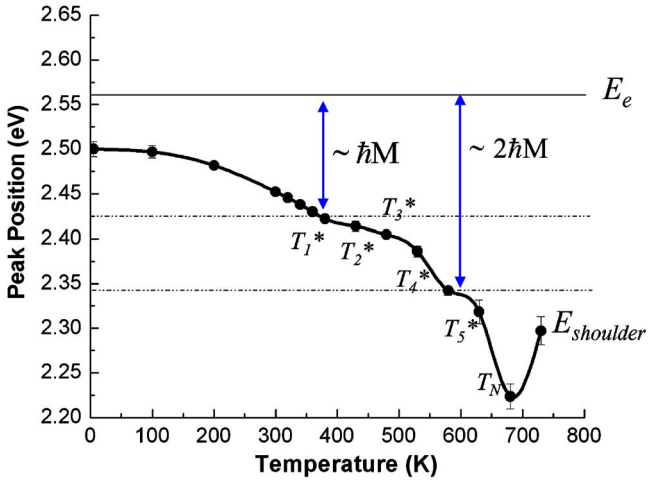

FIG. 5. (Color online) Peak position of the $E_{shoulder}$ as a function of temperature. Also shown are resonance conditions at T_i^* ($i = 1-5$) and T_N involving the electronic level $E_e = 2.56$ eV one- ($1\hbar M$) and two- ($2\hbar M$) magnon levels.

VI. CONCLUSIONS

In summary, we have experimentally demonstrated spin-charge coupling through direct optical probing of electronic sidebands due to high-energy magnon excitations using nonlinear optical spectroscopy. The method is complementary to low-temperature linear absorption spectroscopy which reveals magnon sidebands in $BiFeO_3$ only under high magnetic fields. In contrast, nonlinear spectroscopy can resolve magnon sidebands even at room temperature and above, as shown here, due to significantly lower linewidths and larger energy separation in an SHG spectra between resonant fundamental electronic levels. The work highlights the sensitivity of multimagnon nonlinear optical spectroscopy to spin-charge coupling, by demonstrating a coupling term of the type P_sL^2 in multiferroic bismuth ferrite, that exhibits short-range correlation well into the paramagnetic phase. Such probing of coupling should be possible in general in other multiferroics and magnetic systems. Our results present an alternative to magnetic neutron-scattering measurements, es-

pecially in thin-film geometry where the interaction of neutrons with spin waves is weak and can be challenging.

ACKNOWLEDGMENTS

We acknowledge funding from the National Science Foundation under Grant Nos. DMR-0512165, DMR-0507146, DMR-0820404, DMR-0602986, DMR-0520513, and DMR-0520471, the MSD, BES, U.S. Department of Energy under Contract Nos. DE-AC02-05CH11231 and DE-FG02-01ER45885, and the DOE/BES under Contract No. DE-AC02-06CH11357.

[1] R. L. Greene, D. D. Sell, W. M. Yen, A. L. Schawlow, and R. M. White, Phys. Rev. Lett. **15**, 656 (1965).
[2] R. M. White and W. M. Yen, Low Temp. Phys. **31**, 777 (2005).
[3] The antiresonant *term* can be neglected under near-resonant conditions.
[4] M. Fiebig, V. V. Palov, and R. V. Pissarev, J. Opt. Soc. Am. B **22**, 96 (2005).
[5] S. Denev, A. Kumar, M. Biegalski, H. W. Wang, C. M. Folkman, A. Vasudevarao, Y. Han, I. M. Reaney, S. T. Mckinstry, C. B. Eom, D. G. Scholm, and V. Gopalan, Phys. Rev. Lett. **100**, 257601 (2008).
[6] P. Fischer and F. Hache, Chirality **17**, 421 (2005).
[7] M. Fiebig, D. Fröhlich, K. Kohn, St. Leute, Th. Lottermoser, V. V. Pavlov, and R. V. Pisarev, Phys. Rev. Lett. **84**, 5620 (2000).
[8] D. Frohlich, S. Leute, V. V. Pavlov, and R. V. Pisarev, Phys. Rev. Lett. **81**, 3239 (1998).
[9] A. B. Sushkov, M. Mostovoy, R. Valdes Aguilar, S.-W. Cheong, and H. D. Drew, J. Phys. Condens. Matter **20**, 434210 (2008).
[10] M. Cazayous, Y. Gallais, A. Sacuto, R. de Sousa, D. Lebeugle, and D. Colson, Phys. Rev. Lett. **101**, 037601 (2008).
[11] M. K. Singh, R. S. Katiyar, and J. F. Scott, J. Phys.: Condens. Matter **20**, 252203 (2008).
[12] M. G. Cottam and D. J. Lockwood, *Light Scattering in Magnetic Solids* (Wiley, New York, 1976).
[13] J. D. Perkins, J. M. Graybeal, M. A. Kastner, R. J. Birgeneau, J. P. Falck, and M. Greven, Phys. Rev. Lett. **71**, 1621 (1993).
[14] R. S. Meltzer, M. Lowe, and D. S. McClure, Phys. Rev. **180**, 561 (1969).
[15] R. White, Low Temp. Phys. **31**, 777 (2005).
[16] J. B. Parkinson, J. Phys. C **2**, 2012 (1969).
[17] K. Eguchi, Y. Tanabe, T. Ogawa, M. Tanaka, Y. Kawabe, and E. Hanamura, J. Opt. Soc. Am. B **22**, 128 (2005).
[18] Y. Ogawa, Y. Kaneko, J. P. He, X. Z. Yu, T. Arima, and Y. Tokura, Phys. Rev. Lett. **92**, 047401 (2004).
[19] J. S. Dodge, A. B. Schumacher, J. Y. Bigot, D. S. Chemla, N. Ingle, and M. R. Beasley, Phys. Rev. Lett. **83**, 4650 (1999).
[20] X. S. Xu, T. V. Brinzari, S. Lee, Y. H. Chu, L. W. Martin, A. Kumar, S. Macgill, R. C. Rai, R. Ramesh, V. Gopalan, S. W. Cheong, and J. L. Musfeldt, Phys. Rev. B **79**, 134425 (2009).
[21] D. Lebeugle, D. Colson, A. Forget, M. Viret, P. Bonville, J. F. Marucco, and S. Fusil, Phys. Rev. B **76**, 024116 (2007).
[22] F. Kubel and H. Schmid, Acta Crystallogr., Sect. B: Struct. Sci. **B46**, 698 (1990).
[23] P. Fischer, M. Polomska, I. Sosnowska, and M. Szymanski, J. Phys. C **13**, 1931 (1980).
[24] R. Haumont, J. Kreisel, P. Bouvier, and F. Hippert, Phys. Rev. B **73**, 132101 (2006).
[25] T. Zhao, A. Scholl, F. Zavaliche, K. Lee, M. Barry, A. Doran, M. P. Cruz, Y. H. Chu, C. Ederer, N. A. Spaldin, R. R. Das, D. M. Kim, S. H. Baek, C. B. Eom, and R. Ramesh, Nature Mater. **5**, 823 (2006).
[26] M. O. Ramirez, M. Krishnamurthi, S. Denev, A. Kumar, S.-Y. Yang, Y.-H. Chu, E. Saiz, J. Seidel, A. P. Pyatakov, A. Bush, D. Viehland, J. Orenstein, R. Ramesh, and V. Gopalan, Appl. Phys. Lett. **92**, 022511 (2008).
[27] M. J. Massey, U. Baier, R. Merlin, and W. H. Weber, Phys. Rev. B **41**, 7822 (1990).
[28] S. J. Clark and J. Robertson, Appl. Phys. Lett. **90**, 132903 (2007).
[29] J. B. Neaton, C. Ederer, U. V. Waghmare, N. A. Spaldin, and K. M. Rabe, Phys. Rev. B **71**, 014113 (2005).
[30] G. E. Jellison and F. A. Modine, Appl. Phys. Lett. **69**, 2137 (1996).
[31] R. W. Collins and A. S. Ferlauto, in *Handbook of Ellipsometry*, edited by H. G. Tompkins and E. A. Irene (William Andrew, Norwich, NY, 2005), pp. 159–171.
[32] K. A. Wickersheim and R. A. Lefever, J. Chem. Phys. **36**, 844 (1962).
[33] M. K. Singh, H. M. Jang, S. Ryu, and M. Jo, Appl. Phys. Lett. **88**, 042907 (2006).
[34] M. J. Massey, U. Baier, R. Merlin, and W. H. Weber, Phys. Rev. B **41**, 7822 (1990).
[35] M. O. Ramirez, A. Kumar, S. A. Denev, Y. H. Chu, J. Seidel, L. W. Martin, S.-Y. Yang, R. C. Rai, X. S. Xu, J. F. Ihlefeld, N. J. Podraza, E. Saiz, S. Lee, J. Klug, S. W. Cheong, M. J. Bedzyk, O. Auciello, D. G. Schlom, J. Orenstein, R. Ramesh, J. L. Musfeldt, A. P. Litvinchuk, and V. Gopalan, Appl. Phys. Lett. **94**, 161905 (2009).
[36] J. F. Ihlefeld, A. Kumar, V. Gopalan, D. G. Schlom, Y. B. Chen, X. Q. Pan, T. Heeg, J. Schubert, X. Ke, P. Schiffer, J. Orenstein, L. W. Martin, Y. H. Chu, and R. Ramesh, Appl. Phys. Lett. **91**, 071922 (2007).
[37] A. Kumar, R. C. Rai, N. J. Podraza, S. Denev, M. Ramirez, Y.-H. Chu, L. W. Martin, J. Ihlefeld, T. Heeg, J. Schubert, D. G. Schlom, J. Orenstein, R. Ramesh, R. W. Collins, J. L. Musfeldt, and V. Gopalan Appl. Phys. Lett. **92**, 121915 (2008).
[38] P. A. Fleury, Phys. Rev. **180**, 591 (1969).
[39] See EPAPS Document No. E-PRBMDO-79-007918 for the Raman experiments. For more information on EPAPS, see http://www.aip.org/pubservs/epaps.html.
[40] A. K. Zvezdin and A. P. Pyatakov, Phys. Usp. **47**, 416 (2004).
[41] D. Sa, R. Valenti, and C. Gros, Eur. Phys. J. B **14**, 301 (2000).
[42] I. Dzyaloshinsky, J. Phys. Chem. Solids **4**, 241 (1958).
[43] T. P. Martin, R. Merlin, D. R. Huffman, and M. Cardona, Solid State Commun. **22**, 565 (1977).
[44] P. A. Fleury and R. Loudon, Phys. Rev. **166**, 514 (1968).
[45] F. Bloch, Z. Phys. **61**, 206 (1930).
[46] S. R. Basu, L. W. Martin, Y. H. Chu, M. Gajek, R. Ramesh, R. C. Rai, X. Xu, and J. L. Musfeldt, Appl. Phys. Lett. **92**, 091905 (2008).